Identification and Control of Magneto-Kinetic Response During Advanced Tokamak Scenarios in DIII-D

William Wehner, Wenyu Shi, Eugenio Schuster, Didier Moreau, Michael L. Walker, John R. Ferron, Tim C. Luce, David A. Humphreys, Ben G. Penaflor and Robert D. Johnson

***Abstract*— The paper proposes a model-based control approach for the coupled evolution of the poloidal magnetic flux profile and the normalized pressure ratio β_N. The model is determined by a system identification method which is shown to sufficiently reproduce the plasma response to variations in particular actuators. Data for model identification is collected during the plasma current flattop in a large β_N, high-confinement scenario (H-mode) with the actuators modulated in open loop. Using this data, a linear state-space plasma response model for the poloidal magnetic flux profile and β_N dynamics around a plasma equilibrium state is identified. An optimal state feedback controller with integral action is designed for the purpose of simultaneous control of the poloidal flux profile and β_N. Experimental results showing the performance of the proposed controller implemented in the DIII-D tokamak are presented.**

I. Introduction

To initiate a fusion reaction on earth, temperatures on the order of $10^7 - 10^9$ K are required to overcome the Coulomb repulsion between like-charged nuclei. The conventional fusion plasma, i.e., a hot gas of hydrogen ions and electrons, must be confined by magnetic fields because the high temperatures would otherwise melt the confining structure. The motion of ionized particles are tied to the magnetic field lines by the Lorentz force, so, to contain the plasma, the common solution is to close the magnetic field lines in on themselves, forming a torus as shown in Fig. 1. The primary field component, in the longitudinal direction, is called the toroidal field, labeled B_ϕ. The magnetic field component in the azimuthal direction, called the poloidal field, B_θ, serves to counteract the various forces on the plasma due to field curvature and gradient that cause particle drift towards the vessel wall. Following a given field line a number of times around the torus a closed flux tube is mapped, a so called magnetic-flux surface. These surfaces mark points of constant poloidal magnetic flux [1], a collection of such points along the plasma radius is called the poloidal magnetic flux profile, labeled ψ in this work.

The design of an efficient, economically viable tokamak machine will require the development of what's called an advanced tokamak (AT) scenario. The scenario is characterized by an optimization of various plasma parameter profile shapes. Investigations have shown that careful control of some plasma profiles, such as the poloidal magnetic flux profile (ψ-profile), can help stabilize the plasma while reducing transport and enhancing non-inductive current sources necessary for steady-state operation [2], [3], [4] ('profile' refers to the shape that a plasma variable takes as a function of the minor radius, r (see Fig. 1)). AT scenarios require high β_N, a key performance parameter which is defined as the normalized ratio between the internal plasma kinetic pressure and the external pressure of the confining magnetic field. The β_N parameter represents a measure of efficiency of confinement since it defines how much magnetic confining pressure is required to maintain a particular plasma kinetic pressure. This work attempts to model and control the coupled evolution of the ψ and β_N.

System identification (data-driven modeling) using experimental data has been used to model profile dynamics in ASDEX Upgrade [5]. In the JET tokamak [6], a two-time-scale linear model has been used to describe the dynamics of the magnetic and kinetic profiles around certain quasi-steady-state trajectories, where system matrices can be identified from experimental data. Our previous work [7] considered system identification of a low order model of the poloidal flux profile in DIII-D. This work builds upon the previous modeling procedure and extends the model to span the full profile by projecting the measured data onto a low order subspace and limiting identification to the main response dynamics. Moreover, the model is augmented to include the effects of off-axis neutral beam injection, beams that are directed at an angle to the plasma axis, where previously all neutral beams were aligned for on-axis injection.

The aim of the paper is to develop an input-output response model and a real-time feedback controller, for the magnetic profile dynamics and β_N in response to the neutral beams injectors (NBI), electron cyclotron current/heating (EC) H&CD, and the plasma loop voltage during H-mode scenarios in DIII-D. This paper is organized as follows; Section II describes the model structure, available actuators, data collection, and system identification procedure. Based on the obtained linear model an optimal feedback integral controller is designed in Section III to regulate the ψ-profile and β_N around a desired target in the presence of disturbances. Experimental results on DIII-D are presented in Section IV and conclusions made in Section V.

This work was supported in part by the National Science Foundation CAREER Award program (ECCS-0645086) and the U.S. Department of Energy (DE-FG02-09ER55064 and DE-FC02-04ER54698). W. Wehner (wehner@lehigh.edu), W. Shi, and E. Schuster are with the Department of Mechanical Engineering and Mechanics, Lehigh University, Bethlehem, PA 18015, USA. D. Moreau is with CEA, IRFM, 13108 Saint-Paul-lez-Durance, France. M.L. Walker, J.R. Ferron, T.C. Luce, D.A. Humphreys, B.G. Penaflor, and R.D. Johnson are with General Atomics, San Diego, CA 92121, USA.

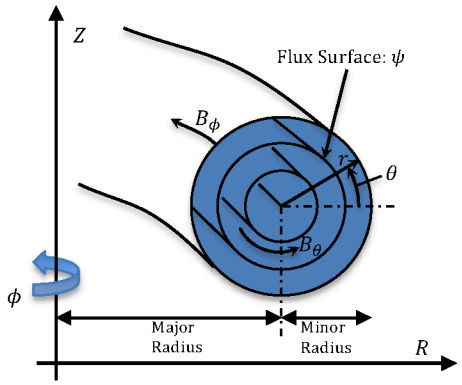

Fig. 1. Magnetic fields of a toroidal confinement system.

II. Model structure and system identification procedure

To collect data for system identification, a number of discharges of an advanced tokamak (AT) scenario (i.e., at high plasma pressure relative to the magnetic field pressure) were run with identical ramp-up phases during the experimental campaign of 2009 [8]. The reference plasma state (equilibrium state) was that of a plasma current $I_p = 0.9$ MA AT scenario which had been optimized to combine non-inductive current fractions near unity with $3.5 < \beta_N < 3.9$, bootstrap current fractions larger than 65%, and $H_{98}(y,2) = 1.5$ [9]. During flattop various actuators were modulated around their reference values. Actuator modulations, at both slow and fast frequencies, were applied from $t = 2.6$ s, i.e., after 1 s of 0.9 MA current flat top.

Available actuators include the neutral beam injectors (NBI), electron cyclotron (EC) power and the plasma surface loop voltage. The NBIs, fast neutrals injected into the bulk plasma, are the primary source of auxiliary heating. Charged particles cannot be injected into the plasma because of the magnetic field, but neutrals can cross the magnetic field and once in the plasma they impart their energy by collisions. The EC power is delivered in the form of radio frequency waves which resonate with the plasma and drive current or create heat. The surface loop voltage is generated by a transformer which is the main source of current drive.

The NBIs were grouped by: co-injection beam power, counter-injection beam power, and balanced-injection beam power, where the co-injection means in the direction of plasma current, counter-injection is the opposing direction, and balanced-injection refers to equal co- and counter-injection power. All actuators were modulated individually in open loop according to predefined waveforms while the other actuators were kept constant and equal to those values used to produce the reference discharge. Starting in 2012, two of the co-injection neutral beam injectors were re-positioned to direct their beams at 16.5° off-axis, providing more current drive towards the center of the profile. Data from the 2012 campaign is used to include the effects of off-axis NBI.

The transport equations describing the time evolution of current density, the plasma density, and temperature of the plasma can be reduced to a 1D model by assuming an axisymmetric plasma and approximating the plasma volume as a long cylinder which reduces the differential operators to derivatives with respect to the radial coordinate alone [6]. Linearizing the resulting set of simplified transport equations around a particular plasma equilibrium state and projecting the plasma parameters onto an appropriate set of basis functions, one can obtain a simple discrete, lumped-parameter model to represent the coupled evolution of the poloidal magnetic flux, $\psi(t)$, and β_N:

$$\frac{\partial \psi}{\partial t} = A\psi + Bu, \text{ and } \beta_N = C_{\beta_N}\psi + D_{\beta_N}u. \quad (1)$$

This work makes uses the mean geometric radius, ρ; it can be expressed in terms of the toroidal magnetic flux, Φ, and the toroidal field strength at the plasma center, $B_{\phi,0}$, i.e. $\pi B_{\phi,0}\rho^2 = \Phi$. Normalized ρ, denoted by $\hat{\rho}$, is defined as ρ/ρ_b, where ρ_b is the value of ρ at the last closed magnetic flux surface. Since the magnetic profile has only a slow evolution, we can use the unfiltered input/output data to identify the model, i.e. all frequencies of the measured data. The measured profile data was first projected onto 9 trial basis functions by Galerkin projection reducing the distributed data set to an approximate discrete data set of 9 points across the normalized plasma radius $\hat{\rho} = 0.1, 0.2, ..., 0.9$. System identification for the discretized ψ-profile was carried out using data collected during experiments in which the various actuators were modulated in open loop. All-in-all, a model of 9 states all measurable, 1 output, and 6 inputs is to be identified by the a step-wise identification procedure described in Sections II-A and II-B.

A. Model order reduction

If we try to identify a model of full order, i.e. an A matrix of size 9×9, the number of parameters becomes rather large. When using noisy experimental data the possible solutions become multiple and unstable to small changes in the data and the identification algorithm cannot determine a consistent model. In order to find a model that applies to all 9 discrete points, the data set has to be projected onto an appropriate subspace of reduced order [10]. Then we identify only the dynamics within this subspace and neglect the remaining dynamics.

For the ψ-profile, the static gain matrix

$$K_{sg} = -A^{-1}B, \quad (2)$$

which represents the steady state gain of the profile in response to a step input for each of the actuators, can be used to determine the subspace since it contains the most essential aspects of the model for control purposes, namely the steady state response. Singular value decomposition of the static gain matrix is used to determine its principal components, the most significant of which are used to form the subspace basis

$$K_{sg} = W \cdot \Sigma \cdot V^T, \quad (3)$$
$$= [W_1\ W_2\ \ldots\ W_{n_y}] \cdot \Sigma \cdot [V_1\ V_2\ \ldots\ V_{n_u}]^T. \quad (4)$$

The output vectors corresponding to the largest singular values are used as the subspace basis. For example, if we

choose to identify a model with order 3, the first three singular vectors, W_1, W_2, and W_3, would form the subspace basis. Thus, the data used for identification would capture the dominant characteristics of the system in steady state. A reduced order model of the form

$$\dot{X}(t) = A_s X(t) + B_s u(t) \tag{5}$$

is then sought by system identification, where $X(t)$ represents the reduced order states, determined by

$$X(t) = \begin{bmatrix} W_1 & W_2 & W_3 \end{bmatrix}^T \psi(t) \triangleq W_s^T \psi(t). \tag{6}$$

Once A_s and B_s have been identified, the system output equation which maps the states, $X(t)$, to the 9 discrete points, $\psi(t)$, is assumed to be $\psi(t) = W_s X(t)$.

B. Model identification procedure

In prior work [7], a model was determined for the ψ-profile at 5 discrete points ($\hat{\rho} = [0.2, 0.4, 0.5, 0.6, 0.8]$), from this model we obtain an initial estimate of the static gain matrix (2) necessary to begin the identification process. The model is then identified using a step-wise approach, meaning parts of the model are identified in one step, then held constant to identify other parts of the model, iterating back and forth until a suitable model is determined. The identification experiments, alternatively referred to as shots, used to generate the model were organized into various groups; one group for shots with little modulation, and one group for each set of shots with modulation in just one of the actuators. We start with the low modulation group to identify the free dynamics of the system, i.e. the matrix A_s. Once the A_s matrix is determined, we identify the B_s matrix one column at a time using shots with only one modulated input corresponding to that B_s column. Then the static gain matrix is updated and the subspace basis is updated for subsequent iterations.

The identification process is carried out using the prediction error method [11] which calculates the matrices A_s and B_s by minimizing the norm $V_N(A_s, B_s) = \frac{1}{N}\sum_{k=1}^{N} \epsilon^2(k)$, where $\epsilon(k)$, called the prediction error, is the difference between the measured output and the predicted output at discrete time k. We begin the identification considering only the data without off-axis NBI. To begin the identification of A_s, a model and subspace of order 1 was chosen to identify the smallest eigenvalue, i.e. the longest characteristic time of the system. This eigenvalue was then held constant and the model order was increased to 2 to identify the next eigenvalue, this process was repeated up to order 4 using the shot group with low input modulation. Then we began with identification of the B_s matrix using the appropriate shot group for each column, while holding the eigenvalues of A_s constant. The identified model was found to have characteristic times of 5.88, 2.38, 1.05, and 0.19 seconds. This means that model orders above 4 have very fast transients with time constants less than 0.19 s, therefore they will not contribute much to the control design and a model of order 4 should be sufficient.

The off-axis NBI deliver a different current drive distribution from that of the on-axis co-injection beams used to identify the model, therefore they must be considered as a new actuator group. To account for this effect an additional column was added to the B_s matrix using various experiments from the early 2012 campaign with similar plasma scenarios to that of the open-loop system identification experiments carried out in 2009. Fig. 2(a) displays an example of the typical fit between the experimental data and the identified model for shot 140094, which included modulation of the NBI power, the EC power, and the external surface loop voltage.

For control purposes it is preferable to have a model that spans the whole profile without an output equation, i.e. one in which the states represent the 9 discrete points of ψ and the outputs are identically the states. The full order model can be achieved by using the subspace basis to expand A_s and B_s while imposing arbitrarily, large stable eigenvalues to the new eigenstates whose dynamics have not been identified. We refer to the new state equation matrices as A and B:

$$A = W_s A_s W_s^T, \; B = W_s B_s. \tag{7}$$

At this point we have obtained a state equation for the ψ-profile of order 9 with 6 inputs, but have yet to consider β_N. The matrices C_{β_N} and D_{β_N} of (1) are estimated in a similar manner as A_s and B_s, first using the shots little input modulation to identify C_s and then identifying D_s column by column using shots with the corresponding input modulated.

The static gain matrix (2) of the identified model can be represented as in Fig. 2(b). In the figure, the steady-state response of the poloidal flux to unitary changes in the various inputs is plotted. The surface loop voltage has the greatest effect in manipulating the profile, the co-injection and counter-injection beams are the second most powerful, affecting the profile in different directions. The contradictory affects of co-injection and counter-injection beams agree with prior experiments considering neutral beam injection at different trajectories [12]. Both the balanced-injection beams and the gyrotrons lead to a small increase in the magnetic profile. The off-axis co-injection beam has a similar effect to the on-axis co-injection beam with the exception of reduced gain on the interior of the profile.

III. Control System Structure

A. Control System Structure

The design of an optimal controller with integral action based on the linear data-driven model identified in Section II is presented in this section. The control algorithm is broken down into two steps: (1) decouple the system and reduce the system to the most relevant control channels (Section III-B) and (2) design the optimal controller based on the reduced system (Section III-C).

The particular plant model under consideration, labeled P, is of the form

$$P : \begin{cases} \dot{x} &= Ax + Bu \\ y &= Cx + Du \end{cases} \tag{8}$$

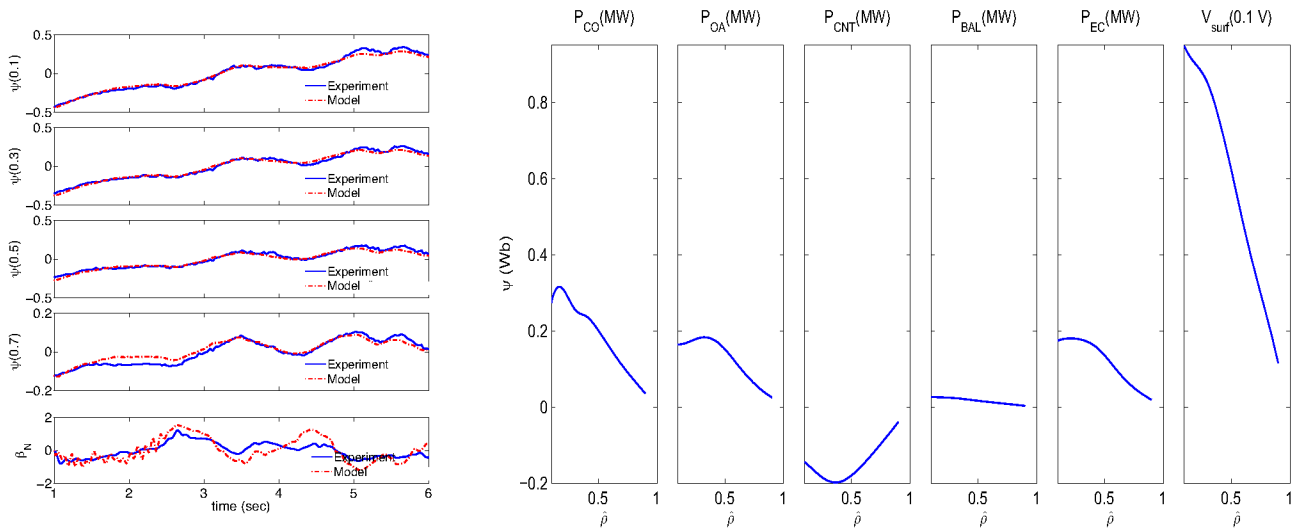

(a) Shot 140094 (b) Static gains

Fig. 2. Left: Comparison between measured (blue) and estimated (red) ψ-profile (Wb) at $\hat{\rho} = 0.1, 0.3, 0.5, 0.7,$ and, 0.9 for DIII-D shot 140094. Right: Model static gain matrix. The powers are the co-current NBI P_{CO} (MW), off-axis co-current NBI P_{OA} (MW), counter-current NBI P_{CNT} (MW), balanced NBI P_{BAL} (MW), electron cyclotron P_{EC} (MW), and surface loop voltage V_{surf} (0.1 V).

where the n model states represent the ψ-profile at the chosen discrete points and the p output measurements y represent the ψ-profile+β_N, i.e. $C = [I_n \; C_{\beta_N}^T]^T$ and $D = [Z_n \; D_{\beta_N}^T]^T$, and Z_n is the zero matrix of size $n \times n$. The vectors $x(t)$, $u(t)$, and $y(t)$ are n-, m-, and p-order, state, control and output vectors, respectively.

B. Singular Value Decomposition

Singular value decomposition is employed to decouple the system and determine the most significant input-output channels for tracking. Provided the closed loop system is internally stable, the steady-state input-output relation can be described by the static gain matrix, $K_{sg} = -CA^{-1}B + D$,

$$\bar{y} = K_{sg}\bar{u}, \tag{9}$$

where $(\bar{\cdot})$ denotes the steady-state value. Consider the singular value decomposition of the weighted static gain matrix

$$\tilde{K}_{sg} = Q^{1/2}K_{sg}R^{-1/2} = U\Sigma V^T \tag{10}$$

where $\Sigma = diag(\sigma_1, \sigma_2, ..., \sigma_m) \in \mathbb{R}^{m\times m}$ for $m \leq p$, $U \in \mathbb{R}^{p\times m}$, $V \in \mathbb{R}^{m\times m}$, and σ_i are the individual singular values with $\sigma_1 > \sigma_2 > ... > \sigma_m$. The positive definite matrices $Q \in \mathbb{R}^{p\times p}$ and $R \in \mathbb{R}^{m\times m}$ are introduced to weight the tracking error and steady-state control effort, respectively. Then the steady state output relation can be expressed as

$$\bar{y} = Q^{-1/2}\tilde{K}_{sg}R^{1/2}\bar{u} = Q^{-1/2}U\Sigma V^T R^{1/2}\bar{u}. \tag{11}$$

The columns of the matrix $Q^{-1/2}U\Sigma$ define a basis for subspace of obtainable steady state output values. Therefore the components of the output signal that are achievable can be defined as

$$\bar{z} = \Sigma^{-1}U^T Q^{1/2}\bar{y} \triangleq K_y\bar{y}. \tag{12}$$

Similarly, the components of the reference that are trackable can be expressed as

$$\bar{r}^* = \Sigma^{-1}U^T Q^{1/2}\bar{r} = K_y\bar{r}. \tag{13}$$

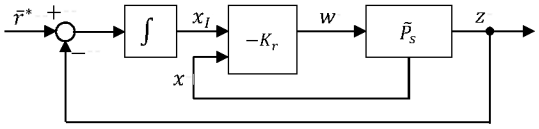

Fig. 3. LQR control configuration with integral action and reference input.

Making use of equations (9), (10) and (12)

$$\begin{aligned} \bar{z} &= \Sigma^{-1}U^T Q^{1/2}\bar{y} \\ &= \Sigma^{-1}U^T Q^{1/2}Q^{-1/2}U\Sigma V^T R^{1/2}\bar{u} \\ &= V^T R^{1/2}\bar{u} \triangleq K_u^{-1}\bar{u}. \end{aligned} \tag{14}$$

If we define $\bar{w}$,

$$\bar{w} = V^T R^{1/2}\bar{u} = K_u^{-1}\bar{u}, \tag{15}$$

then we will have reduced the steady-state plant to a one-one relationship between inputs and outputs, i.e. $\bar{z} = \bar{w}$, which represents a square $m \times m$ decoupled system. Let us define the steady-state performance index as

$$\bar{J} = \lim_{t\to\infty} e^T(t)Qe(t) = \bar{e}^T Q\bar{e}, \tag{16}$$

where $\bar{e}$ is the steady-state tracking error, which can now be rewritten as

$$\bar{e} = \bar{r} - \bar{y} = Q^{-1/2}U\Sigma(\bar{r}^* - \bar{z}) \tag{17}$$

and substituted into (16), resulting in the performance index

$$\bar{J} = (\bar{r}^* - \bar{z})^T\Sigma^2(\bar{r}^* - \bar{z}) = \sum_{i=1}^{m}\sigma_i^2(\bar{r}_i^* - \bar{z}_i)^2. \tag{18}$$

Clearly, the input-output channels associated with the largest singular values are the most significant when minimizing $\bar{J}$. Considering only the largest singular values and ignoring the others by reducing the system appropriately we can significantly reduce the control effort necessary to reach the steady-state target profile without substantial increase in

the steady-state error [13]. The system is reduced to these important channels and the others are ignored. The reduction is carried out using the following partitions:

$$U = [U_s \;\; U_{ns}], \;\; V = [V_s \;\; V_{ns}],$$
$$\Sigma = \begin{bmatrix} \Sigma_s & 0 \\ 0 & \Sigma_{ns} \end{bmatrix} \approx \begin{bmatrix} \Sigma_s & 0 \\ 0 & 0 \end{bmatrix}, \tag{19}$$

where s stands for significant and ns stands for non-significant. Then, from (12), (15), we can approximate

$$\bar{y} = Q^{-1/2} U \Sigma \bar{z} \approx Q^{-1/2} U_s \Sigma_s \bar{z} \triangleq K_{y,s}^{-1} \bar{z}, \tag{20}$$
$$\bar{w} = V^T R^{1/2} \bar{u} \approx V_s^T R^{1/2} \bar{u} \triangleq K_{u,s}^{-1} \bar{u}. \tag{21}$$

Defining $z = K_{y,s} y$ and $u = K_{u,s} w$, we can write

$$z = K_{y,s} P K_{u,s} w \triangleq \tilde{P}_s w, \tag{22}$$

where we have used the fact that $y = Pu$, $K_{y,s} = \Sigma_s^{-1} U_s^T Q^{1/2}$, $K_{u,s} = R^{-1/2} V_s$ and let s denote the number of significant singular values. The reduced plant is characterized by the state space representation

$$\tilde{P}_s : \begin{cases} \dot{x} = \tilde{A}x + \tilde{B}w \\ z = \tilde{C}x + \tilde{D}w \end{cases} \tag{23}$$

where $\tilde{A} = A$, $\tilde{B} = BK_{u,s}$, $\tilde{C} = K_{y,s}C$, and $\tilde{D} = K_{y,s}DK_{u,s}$.

C. Optimal State Feedback Controller

The control design considers an optimal state feedback controller with integral action added as shown in Fig. 3 to remove the steady-state error. Here the control error $\bar{r}^* - z$ is integrated and the controller is designed for the augmented plant with the integrator states. Adding the integrator states, $x_I = \int \bar{r}^* - z$, to the reduced plant $\tilde{P}$, the augmented plant $(\hat{A}, \hat{B})$ can be expressed as:

$$\dot{\hat{x}} = \begin{bmatrix} 0 & -\tilde{C} \\ 0 & \tilde{A} \end{bmatrix} \hat{x} + \begin{bmatrix} -\tilde{D} \\ \tilde{B} \end{bmatrix} w + \begin{bmatrix} 1 \\ 0 \end{bmatrix} \bar{r}^* \tag{24}$$

with augmented states $\hat{x} = [x_I \; x]^T$.

The task of the control synthesis is to find the optimal control law $w(t) = f(\hat{x}(t))$ which minimizes the following cost functional J [14],

$$J = \lim_{T \to \infty} \frac{1}{T} \int_0^T \left[\hat{x}^T \hat{Q} \hat{x} + w^T \hat{R} w \right] dt, \tag{25}$$

where $\hat{Q}$ is a $n \times n$ symmetric positive-semidefinite matrix and $\hat{R}$ is a $m \times m$ symmetric positive-definite matrix. The solution to this linear quadratic regulator problem (LQR) can be written in terms of the simple state feedback law

$$w(t) = -K_r \hat{x}(t) \tag{26}$$

where K_r is a constant matrix independent of plant noise, given by

$$K_r = \hat{R}^{-1} \hat{B}^T X, \tag{27}$$

where $X = X^T \geq 0$ is the unique positive-semidefinite solution of the algebraic Riccati equation

$$\hat{A}^T X + X \hat{A} - X \hat{B} \hat{R}^{-1} \hat{B}^T X + \hat{Q} = 0. \tag{28}$$

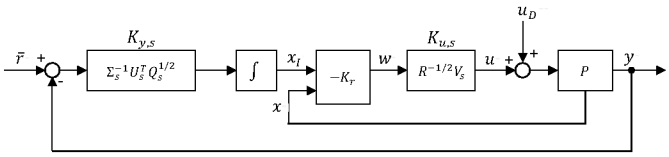

Fig. 4. Overall feedback scheme.

We choose $\hat{Q}$ such that only the integrated states $\int \bar{r} - y$ are weighted, which gives $\hat{Q} = \begin{bmatrix} I_n & 0 \\ 0 & 0 \end{bmatrix}$, and we choose $\hat{R} = \alpha I_m$, with $\alpha > 0$. Note that only the ratio between $\hat{R}$ and $\hat{Q}$ affects the minimum of the cost function, reducing $\hat{R}$ yields a faster response with more control energy.

The control configuration of Fig. 3 can be re-expressed in the form of Fig. 4 to determine the overall controller. The result is the two degree of freedom controller $\tilde{K}$. Using the relation

$$w = -K_r \begin{bmatrix} x_I \\ x \end{bmatrix} \triangleq \begin{bmatrix} -K_I & -K_P \end{bmatrix} \begin{bmatrix} x_I \\ x \end{bmatrix}, \tag{29}$$

and absorbing the integrator, $\tilde{K}$ can be written as

$$\tilde{K} : \begin{cases} \dot{x}_I = 0 x_I + \begin{bmatrix} K_{y,s} & -K_{y,s} \end{bmatrix} \begin{bmatrix} \bar{r} \\ y \end{bmatrix}, \\ u = -K_{u,s} K_I x_I - K_{u,s} \begin{bmatrix} 0_{s \times p} & K_P & 0_1 \end{bmatrix} \begin{bmatrix} \bar{r} \\ y \end{bmatrix}, \end{cases} \tag{30}$$

where K_I is the state feedback matrix for the integrated states and K_P is the state feedback for the original states.

IV. Experimental Results

Using the identified model of Section II, the proposed optimal control law synthesized in Section III was put to the test in experiment at DIII-D. The first two singular values are found to be the most significant and the system is reduced to 2×2 in the singular value decomposition. The weight $\hat{Q}$ is selected such that only the integrator states are weighted in the control design, weighting the 1^{st} integrated state twice as high as the 2^{nd}, and α in $\hat{R}$ is selected such that the system reacts sufficiently quickly without too much overshoot. During the experiment the device was setup to reproduce the initial ramp-up profile of the reference discharge used in Section II for system identification.

Some tuning was done in simulation and eventually the SVD weighting matrices were selected as $Q = diag\{1\}$, $R = diag\{400, 1, 1, 1, 1\}$. The first value of 400 for R was selected to reduce the control effort applied to the surface loop voltage, this large value was chosen to ensure that control requested value was within the physical ramp limits. The multiplier α was set to 0.1 for the controller weight $\hat{R}$.

Fig. 5 shows the resulting inputs and outputs (ψ-profile evolution and β_N value) of the experimental shot 150752. The experimental goal was to reproduce the profile shape and high β_N achieved in shot 147634, an AT scenario shot with high $\beta_N = 3.5$. However, to avoid complete saturation of the all the beam powers and allow some room for profile control, the target β_N of 3.5 was reduced to 3. One of the counter-injection neutral beam-lines was non-operational

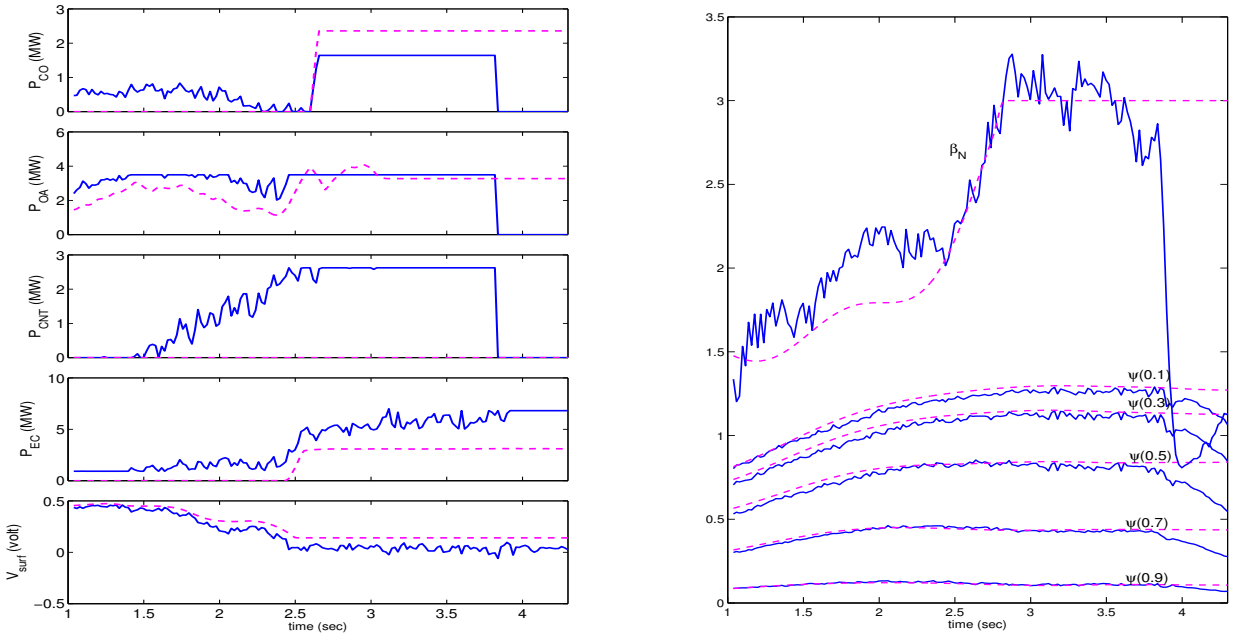

(a) Input Powers

(b) ψ+β_N

Fig. 5. Shot 150752: The green dashed line represents the target profile and associated feed-forward inputs. The blue line represents the control requested inputs during experiment and the measured ψ-profile at $\hat{\rho} = [0.1, 0.3, 0.5, 0.7, 0.9]$ and β_N.

during the experiment, so, the option to use balance injection was not available. The controlled actuators are the on-axis co-injection, off-axis co-injection, on-axis counter-injection neutral beams, the total EC power, and the surface loop voltage. The ψ-profile+β_N controller took over at $t = 1$ s and effectively regulated the ψ-profile around the target profile and drove β_N to the target value. The NBI powers, particularly the counter NBI, are driven up from the feed-forward values to boost the β_N while the V_{surf} value is reduced to balance the increasing beam powers and maintain tight profile regulation. However at $t = 3.5$ s the shot incurred significant magneto-hydro-dynamic activity in the form of a neoclassical tearing mode (NTM). This unfortunate event instigated a controlled termination of the plasma at $t = 3.5$ s. The NTM was most likely caused by the large ramp-up in the co-injection neutral beam power required to achieve the high β_N value.

V. Summary and Conclusions

A simplified linear model for the evolution of the poloidal magnetic flux profile as well as β_N in the DIII-D tokamak was obtained based on a semi-interactive system identification method. Reasonable model prediction of the magnetic profile evolution in response to modulations in the on-axis and off-axis neutral beam injector power, the total gyrotron power, and the surface loop voltage was achieved. An optimal feedback controller with integral action was proposed for tracking a desired target profile and maintaining plasma pressure. During experiment good profile tracking was observed, however, the required large neutral beam powers initiated an NTM, which creates an interest for simultaneous profile and NTM control [15].

References

[1] A. Pironti and M. Walker, "Fusion, tokamaks, and plasma control," *IEEE Control System Magazine*, vol. 25, no. 5, pp. 30–43, 2005.

[2] F. Romanelli and R. Kamendje, "Overview of JET results," *Nucl. Fusion*, vol. 49, no. 104006, 2009.

[3] N. Oyama and for the JT-60 Team, "Overview of JT-60U results towards the establishment of advanced tokamak operation," *Nucl. Fusion*, vol. 49, no. 104007, 2009.

[4] E. Strait and for the DIII-D Team, "DIII-D research in support of ITER," *Nucl. Fusion*, vol. 49, no. 104008, 2009.

[5] Y. S. Na, "Modelling of current profile control in tokamak plasmas," Ph.D. dissertation, Fakultat fur Physik: Technische Universitat Munchen, Munich, Germany, 2003.

[6] D. Moreau *et al.*, "A two time scale dynamic model approach for magnetic and kinetic profile control in advanced tokamak scenarios on JET," *Nucl. Fusion*, vol. 48, no. 106001, 2008.

[7] W. Wehner *et al.*, "Optimal feedback control of the poloidal magnetic flux profile in the DIII-D tokamak based on identified plasma response model," *2012 American Control Conference*, p. 5049, June 2012.

[8] D. Moreau *et al.*, "Plasma models for real-time control of advanced tokamak scenarios," *Nucl. Fusion*, vol. 51, no. 063009, 2011.

[9] C. Holcomb *et al.*, "Optimizing stability, transport, and divertor operation through plasma shaping for steady-state scenario development in DIII-D," *Phys. of Plasmas*, vol. 16, no. 056116, 2009.

[10] D. Moreau *et al.*, "Identification of the magneto-thermal plasma response for plasma state control in advanced tokamaks," *Joint 48th IEEE Conference on Decision and Control and 28th Chinese Control Conference*, p. 1379, Dec. 2009.

[11] L. Ljung, *System Identification: Theory for the User*. Prentice Hall PTR, 1999.

[12] W. Heidbrink *et al.*, "Beam-ion confinement for different injection geometries," *Plasma Physics and Controlled Fusion*, vol. 51, no. 125001, 2009.

[13] G. Ambrosino, M. Ariola, and A. Pironti, "Optimal steady-state control for linear non right-invertible systems," *IET Control Theory and Applications*, vol. 1, no. 3, pp. 604–610, 2007.

[14] S. Skogestad and I. Postlethwaite, *Multivariable Feedback Control*. John Wiley & Sons, West Sussex England, 2005.

[15] W. Wehner and E. Schuster, "Control-oriented modelling for neoclassical tearing mode stabilization via minimum-seeking techniques," *Nucl. Fusion*, vol. 52, no. 074003, 2011.